Supplemental Materials

Molecular Biology of the Cell

Baratam et al.

Supporting Information

Flexible pivoting of dynamin PH-domain catalyzes fission: Insights into molecular degrees of freedom

K. K. Baratam[1†], K. Jha[1†] and A. Srivastava[1*]

[1]Molecular Biophysics Unit, Indian Institute of Science, Bangalore - 560012

Running title: *Dynamics of the membrane-bound dynamin PHD*

† Contributed equally

* To whom correspondence should be addressed: anand@iisc.ac.in

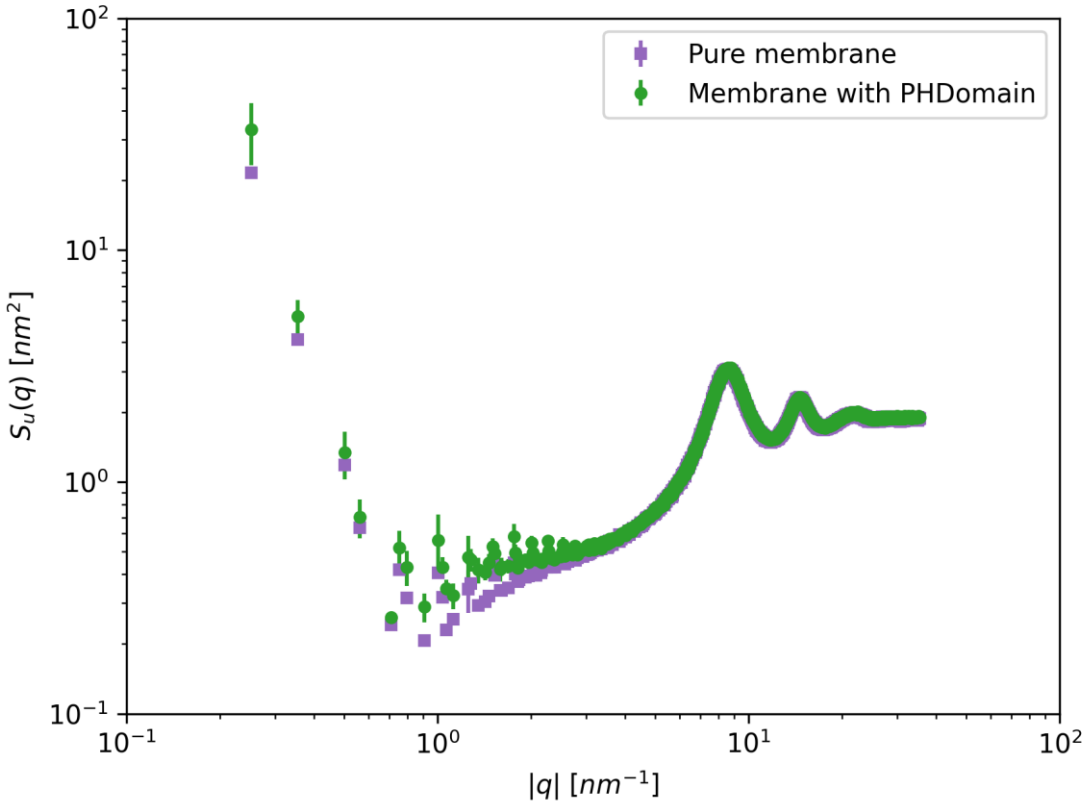

Figure S1: Undulation spectra of CG bilayer (2048 lipids Martini forcefield). Pure bilayer spectra is shown in purple while the spectra with 14 PHDs on the top leaflet (randomly arranged) is shown in green.

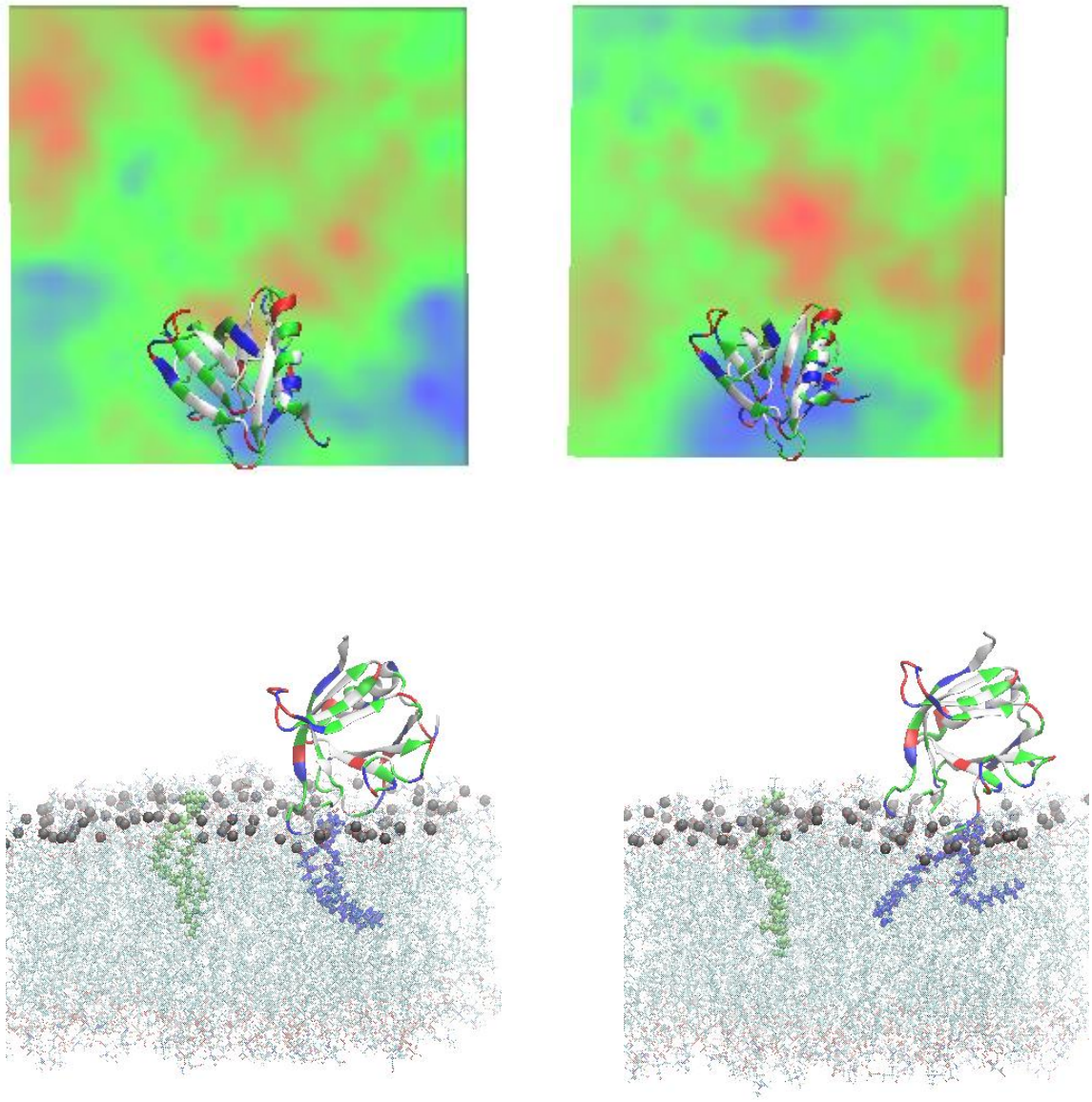

Figure S2: Top panel shows the membrane thickness profile for two other systems with dyn-PHD on all-atom bilayer. The difference between the thinnest and thickest regions is around 0.4 nm. The bottom panel shows snapshot of a PHD-bilayer run and the blue lipid denotes a dyn-PHD proximal lipid while the green color shows the distal lipid. The proximal lipid has a visible tilt (left bottom) and very noticeable splay. The average statistical data for the splay and tilt are shown in Fig. 2.

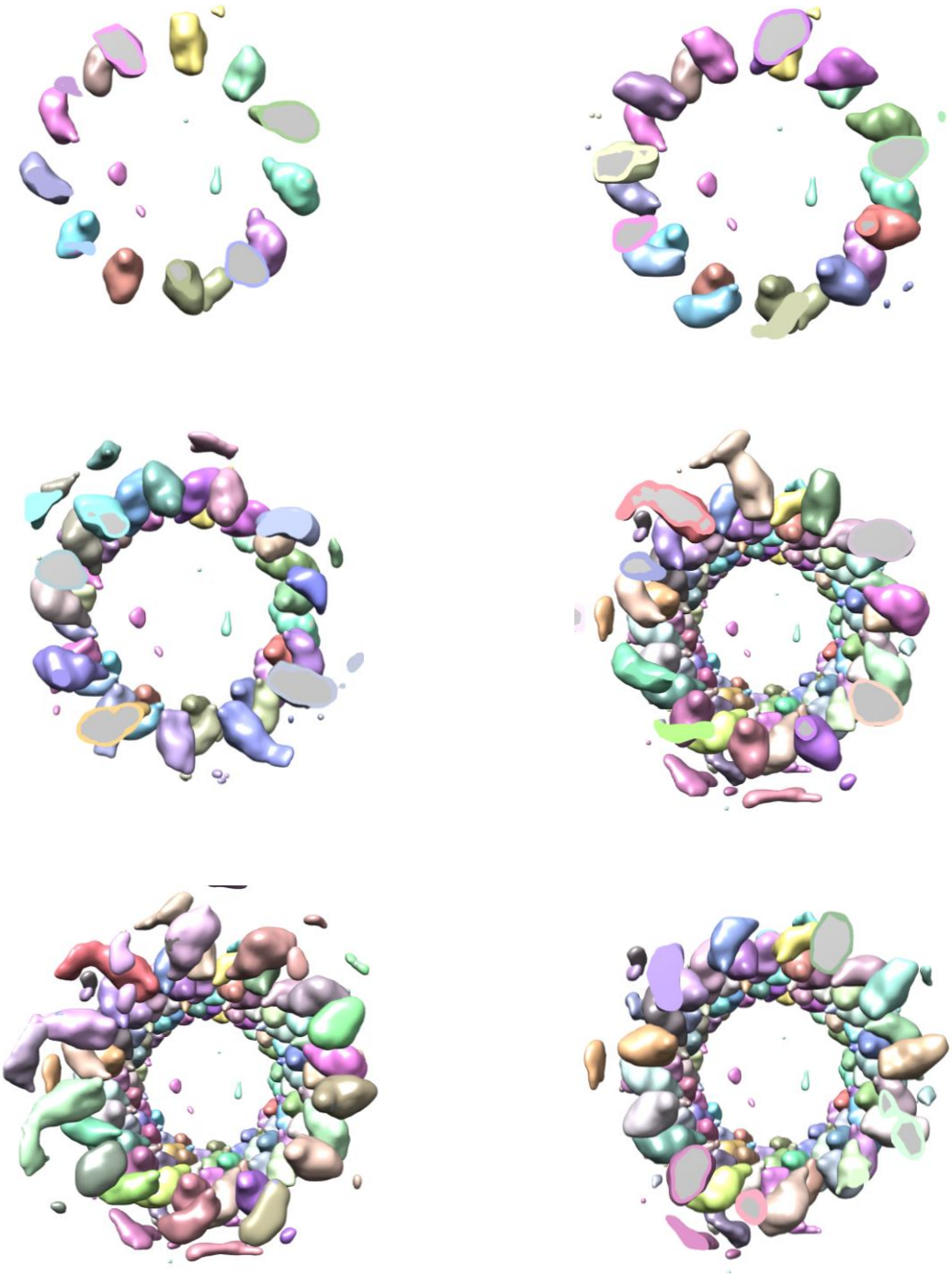

Figure S3: End view of the 3D density map of dynamin polymer assembled on the membrane. The top-left panel shows the front most slice of the scaffold with dyn-PHDs in different orientations. The right-bottom panel shows the full scaffold. The density map is re-drawn from the available cryo-EM density data by Jennifer Hinshaw and co-workers

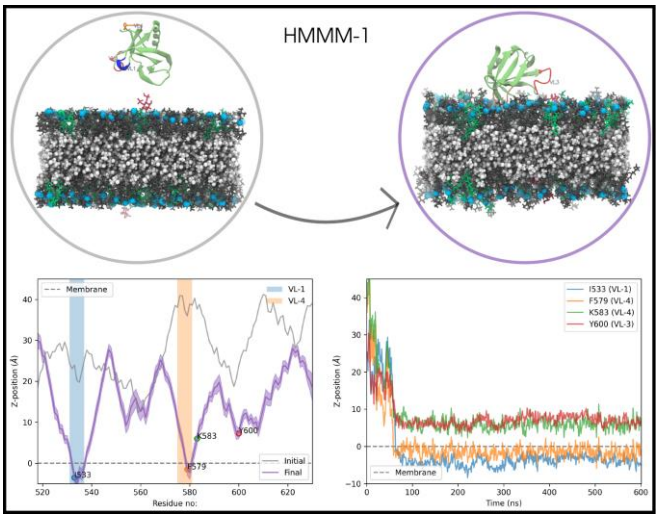
HMMM-1
Membrane
VL-1
VL-4
I533
F579
K583
Y600
Initial
Final
Z-position (Å)
Residue no:
I533 (VL-1)
F579 (VL-4)
K583 (VL-4)
Y600 (VL-3)
Time (ns)

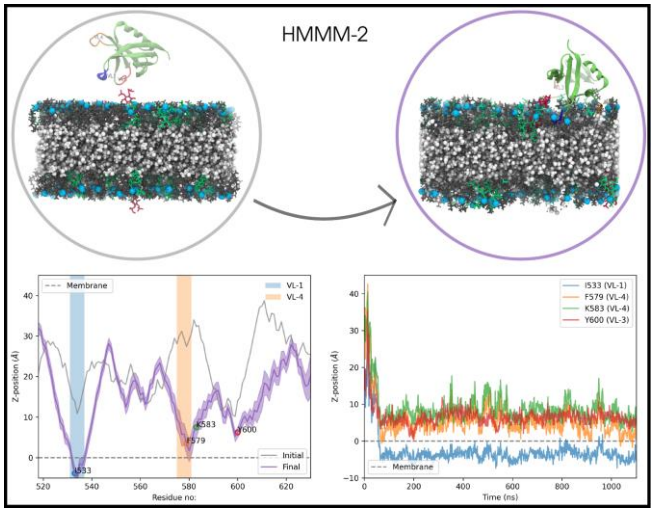
HMMM-2
Membrane
VL-1
VL-4
I533
F579
K583
Y600
Initial
Final
Z-position (Å)
Residue no:
I533 (VL-1)
F579 (VL-4)
K583 (VL-4)
Y600 (VL-3)
Time (ns)

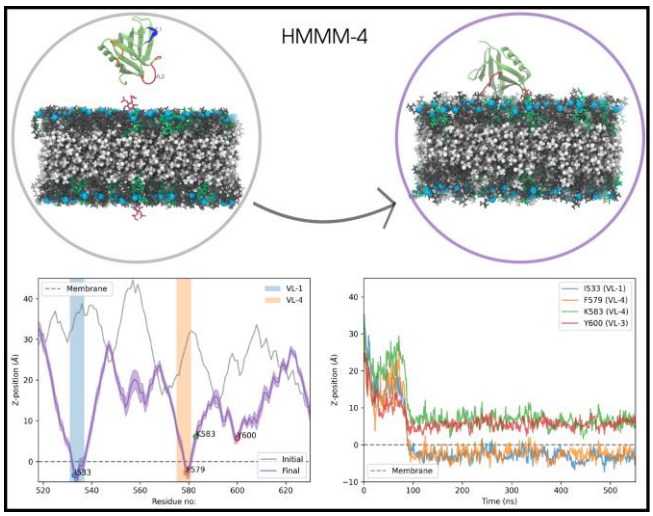
HMMM-4
Membrane
VL-1
VL-4
I533
F579
K583
Y600
Initial
Final
Z-position (Å)
Residue no:
I533 (VL-1)
F579 (VL-4)
K583 (VL-4)
Y600 (VL-3)
Time (ns)

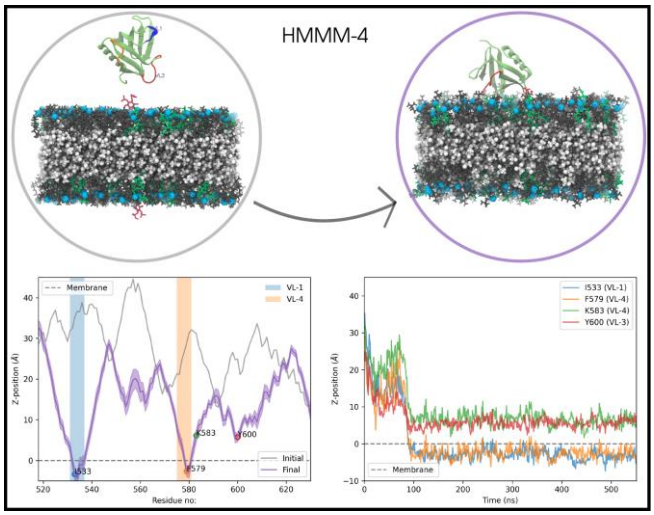
HMMM-4
Membrane
VL-1
VL-4
I533
F579
K583
Y600
Initial
Final
Z-position (Å)
Residue no:
I533 (VL-1)
F579 (VL-4)
K583 (VL-4)
Y600 (VL-3)
Time (ns)

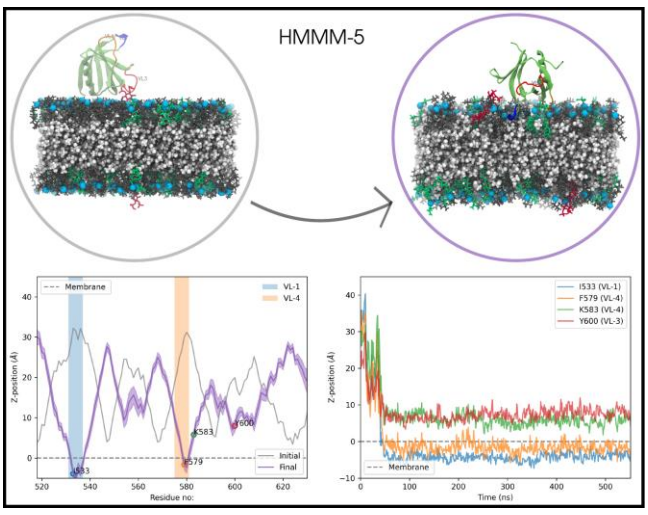
HMMM-5
Membrane
VL-1
VL-4
I533
F579
K583
Y600
Initial
Final
Z-position (Å)
Residue no:
I533 (VL-1)
F579 (VL-4)
K583 (VL-4)
Y600 (VL-3)
Time (ns)

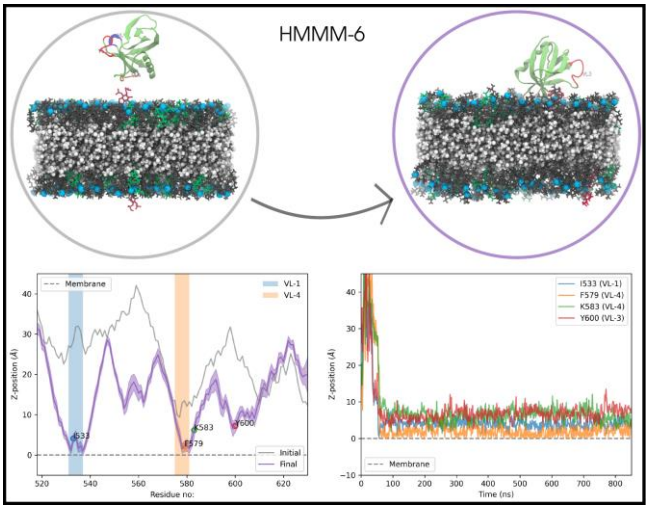
HMMM-6
Membrane
VL-1
VL-4
I533
F579
K583
Y600
Initial
Final
Z-position (Å)
Residue no:
I533 (VL-1)
F579 (VL-4)
K583 (VL-4)
Y600 (VL-3)
Time (ns)

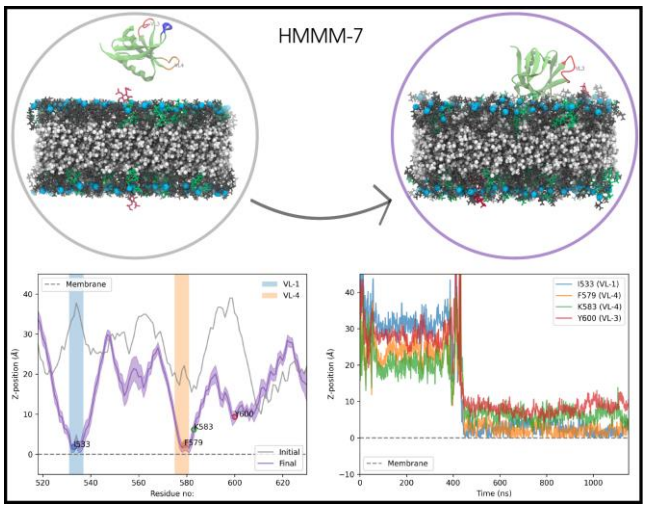

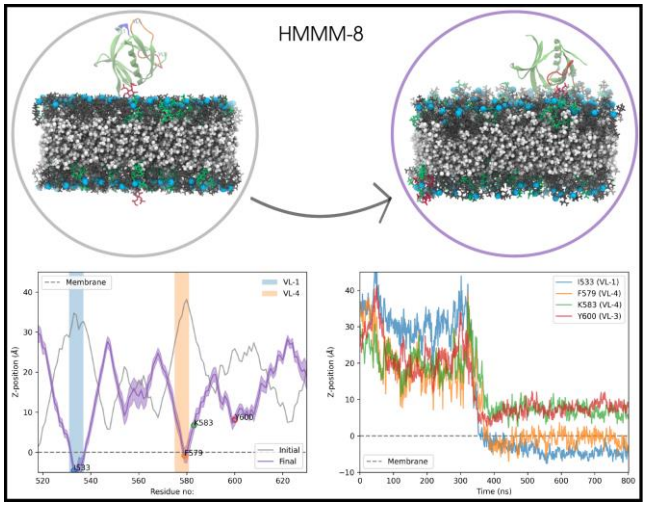

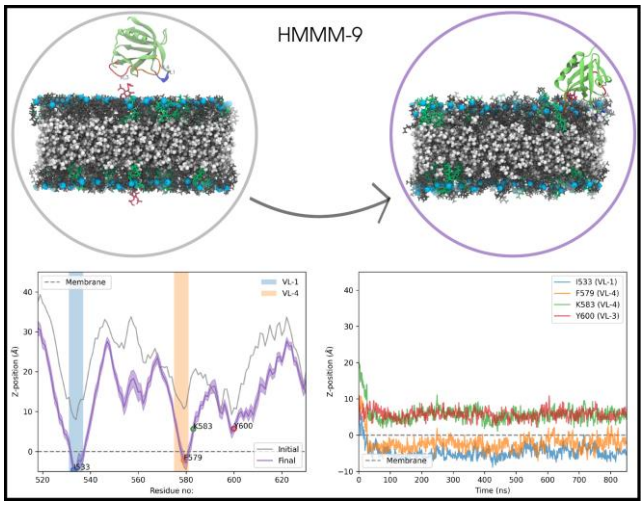

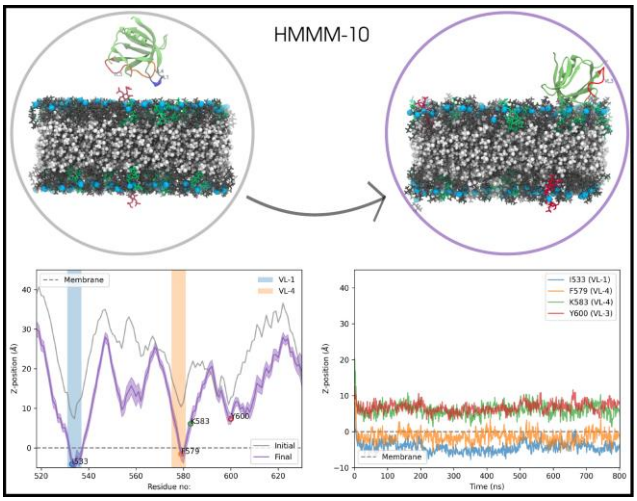

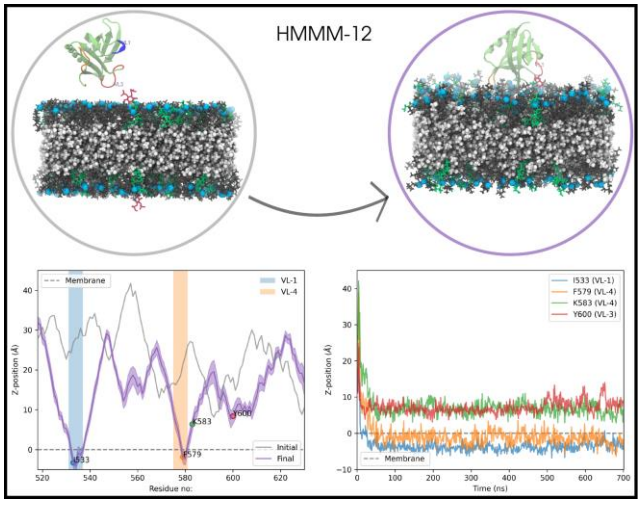

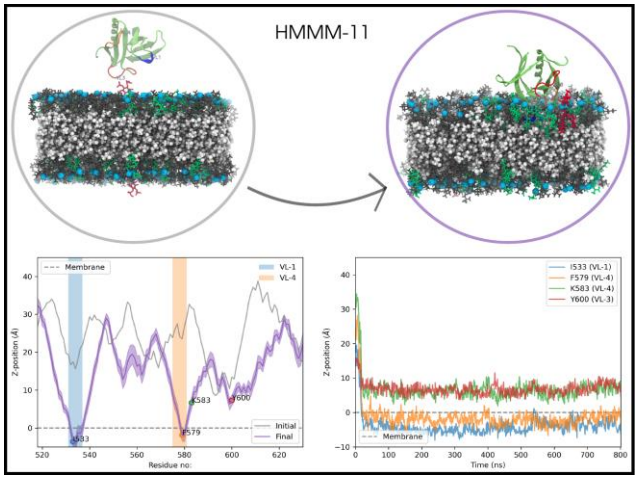

Figure S4: HMMM data for 12 replicates.

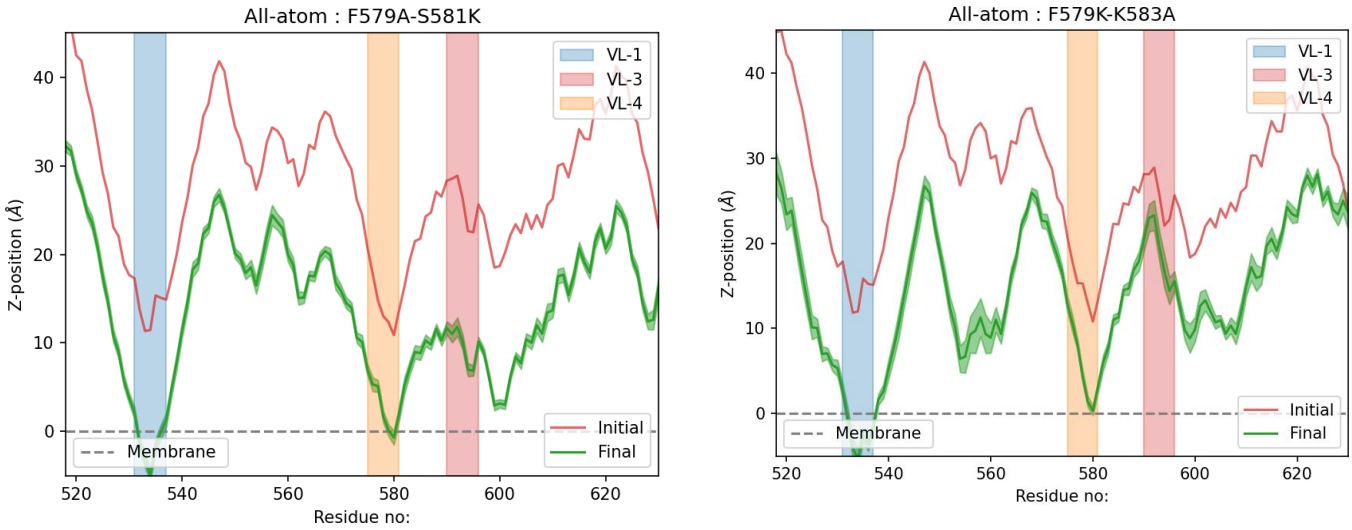

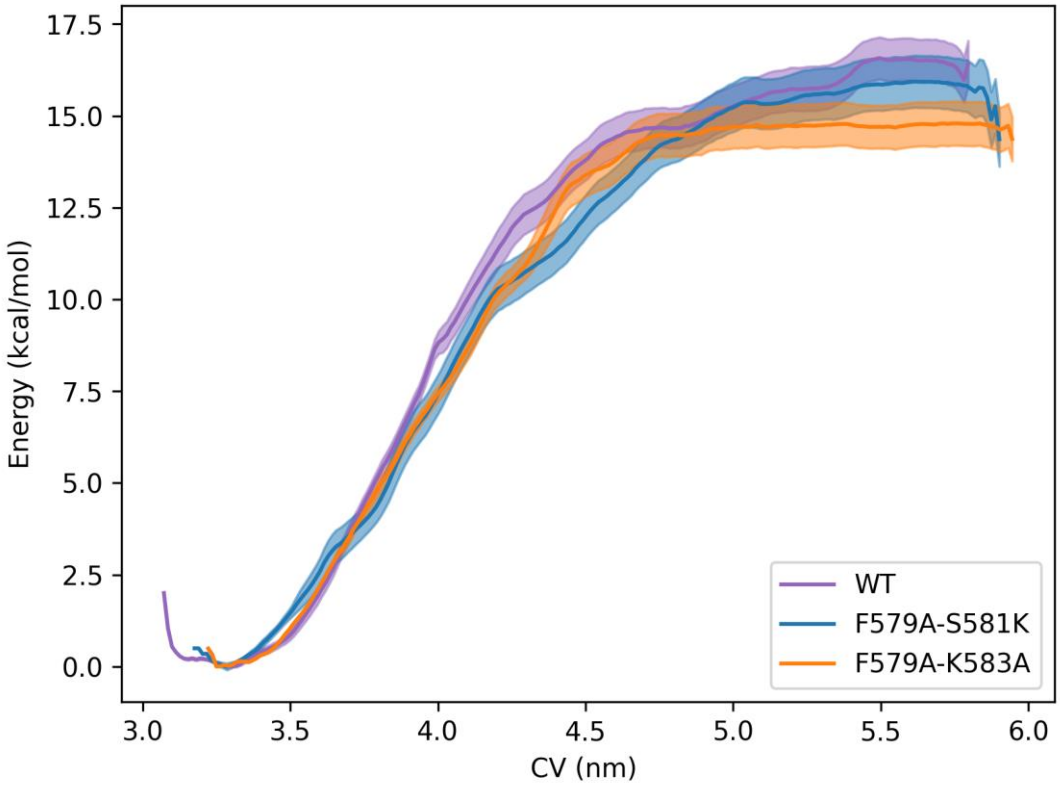

Figure S5: z-distance plots and US PMF data for double mutants

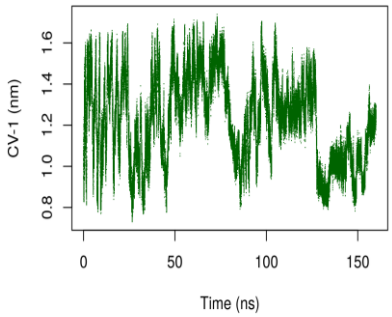
CV-1 (nm)
Time (ns)

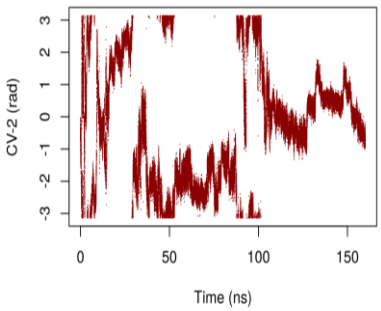
CV-2 (rad)
Time (ns)

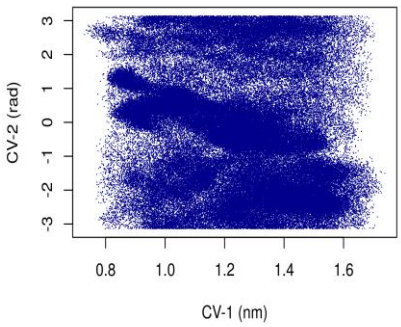
CV-2 (rad)
CV-1 (nm)

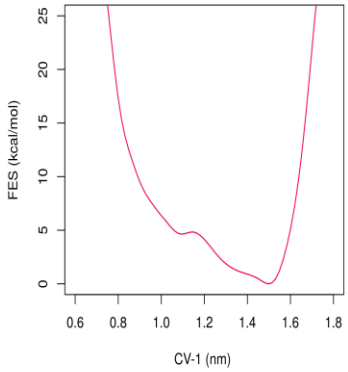
FES (kcal/mol)
CV-1 (nm)

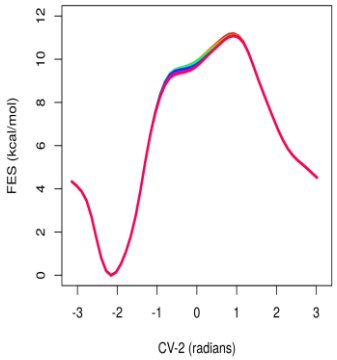
FES (kcal/mol)
CV-2 (radians)

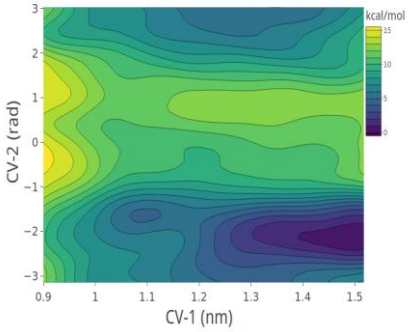
kcal/mol
CV-2 (rad)
CV-1 (nm)

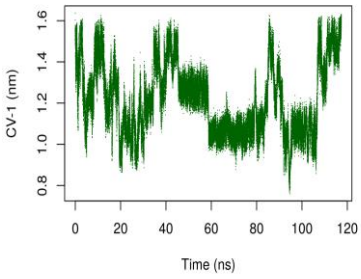
CV-1 (nm)
Time (ns)

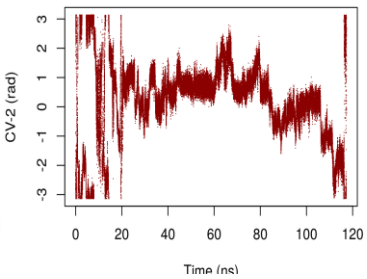
CV-2 (rad)
Time (ns)

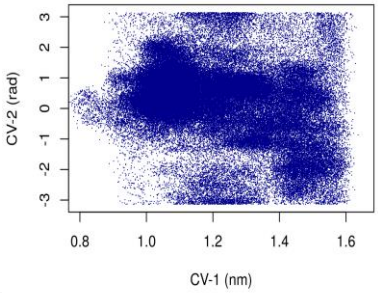
CV-2 (rad)
CV-1 (nm)

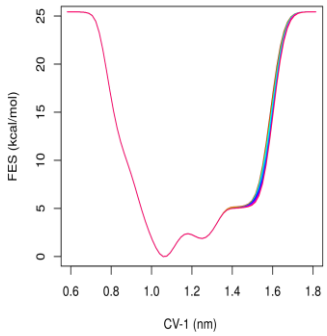
FES (kcal/mol)
CV-1 (nm)

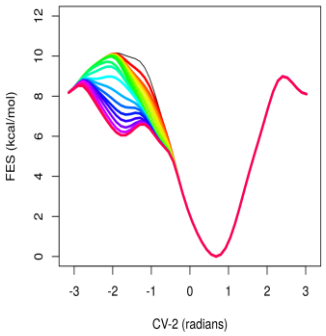
FES (kcal/mol)
CV-2 (radians)

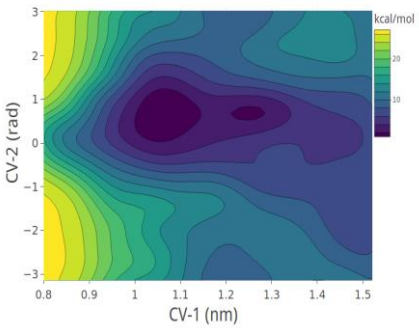
kcal/mol
CV-2 (rad)
CV-1 (nm)

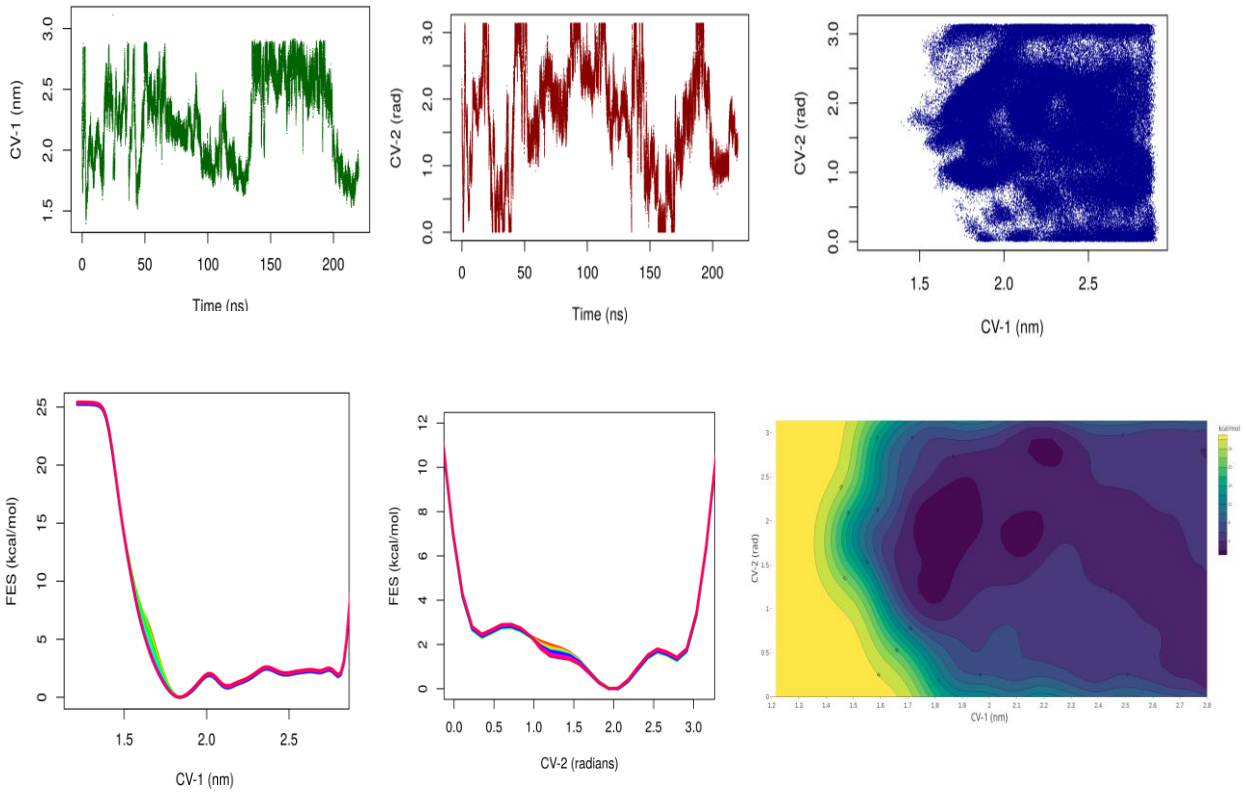

Figure S6: Convergence analysis for the well-tempered metadynamics runs. Top panel shows convergence results for simulations where with VL1-VL3 was chosen as the preferred docking area, middle panel is for system with VL1-VL4 as the preferred pocket and the bottom most panel is for system with no bias for any pocket. Top row for each panel shows the time evolution (sampling) of individual CV as well as both together. The bottom row for each panel shows the free energy surface (FES)data for individual CVs as well as when put together.

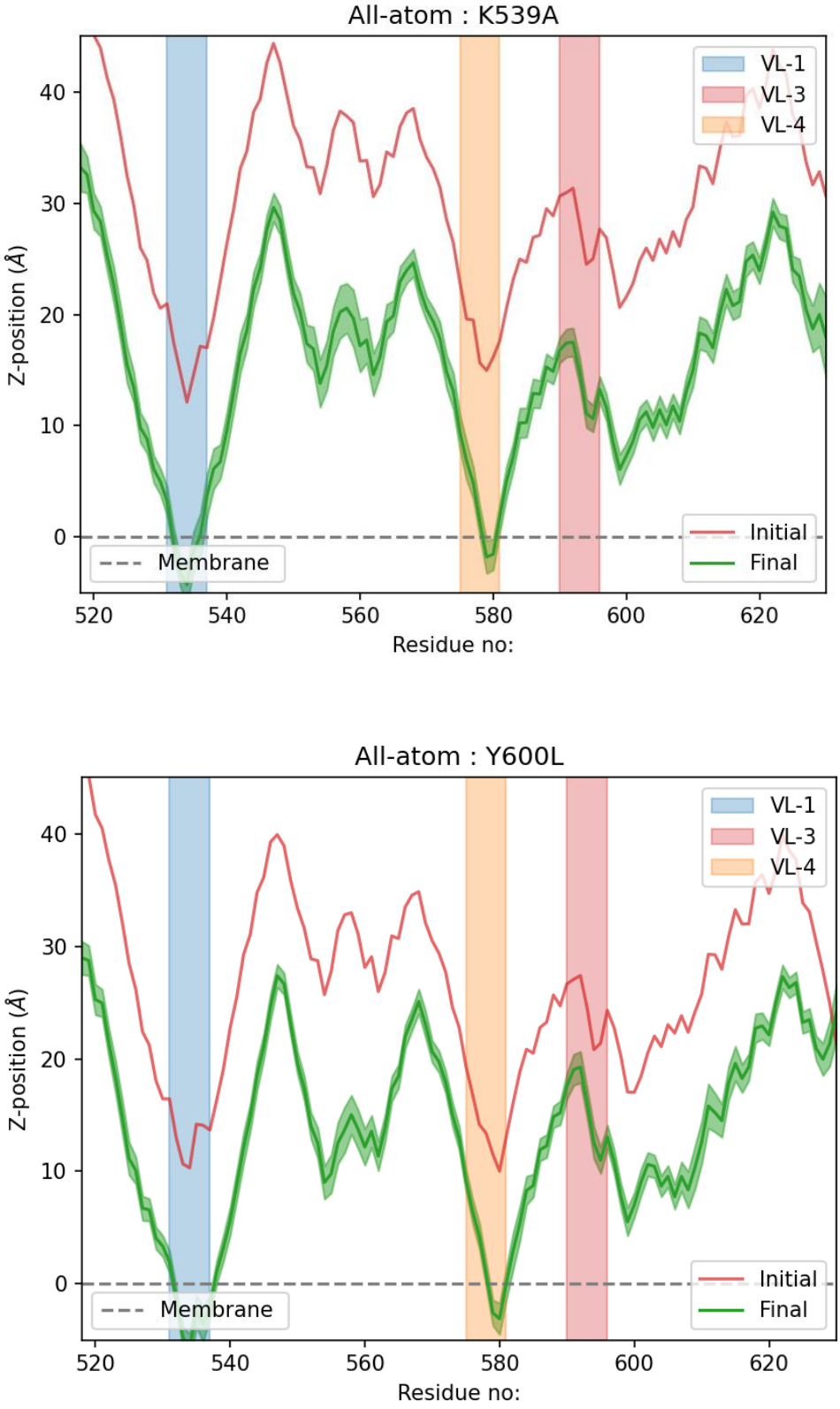

Figure S7: Z-distance analysis for K539A and Y600L from AAMD simulations

1. Well-Tempered Metadynamics Simulation Parameters:

1a. System: Loops 1-3 Well-Tempered metadynamics

Protein: 1DYN (Pleckstrin homology domain)

Ligand: Inositol triphosphate

Definition of CVs

CV1: Distance between centre of mass of ligand's inositol ring and C-alpha atom of residue TYR 600

CV2: Torsion angle (A-B-C-D)

A: C-alpha atom of tyrosine-600

B: C-beta atom of tyrosine-600

C: C2 of inositol ring of ITP

D: C5 of inositol ring of ITP

Metadynamics Parameters:

Initial Height of gaussian: 1.0 kJ/mol
Gaussian deposition rate: 1 ps

Length of the simulation: 160 ns

sigma of gaussian in CV1 direction:0.05 nm

sigma of gaussian in CV2 direction:0.35 rad

CV1 upper restraint: 1.5 nm with harmonic restraint whose kappa=3000

2b. System: Loops 1-4 Well-Tempered metadynamics

Protein: 1DYN (Pleckstrin homology domain)

Ligand: Inositol triphosphate

Definition of CVs:

CV1: Distance between centre of mass of ligand's inositol ring and C-alpha atom of residue

586 (phenylalanine)

CV2: Torsion angle (A-B-C-D)

A: N atom of phenylalanine 586

B: C-alpha atom of phenylalanine 586

C: C2 of inositol ring of ITP

D: C5 of inositol ring of ITP

Metadynamics Parameters:

Initial Height of gaussian: 1.0 kJ/mol

Gaussian deposition rate: 1 ps

Length of the simulation: 110 ns

sigma of gaussian in CV1 direction:0.05 nm

sigma of gaussian in CV2 direction:0.35 rad

CV1 upper restraint: 1.5 nm with harmonic restraint whose kappa=3000

2c. System: Whole Protein Well-Tempered metadynamics

Protein: 1DYN (Pleckstrin homology domain)

Ligand: Inositol triphosphate

Definition of CVs:

CV1: distance between the centroid of protein and the centroid of ligand's inositol ring

CV2: Angle (A-B-C)

A: Centroid of the protein

B: C1 of inositol ring of ITP

C: C4 of inositol ring of ITP

Metadynamics Parameters:

Initial Height of gaussian: 1.0 kJ/mol

Guassian deposition rate: 1 ps

Length of the simulation: 220 ns

sigma of gaussian in CV1 direction:0.05 nm

sigma of gaussian in CV2 direction:0.35 rad

CV1 lower restraint: 1.2 nm with harmonic restraint whose kappa=2000

CV1 upper restraint: 2.8 nm with harmonic restraint whose kappa=2000

2. Justification for using PHD instead of dynamin: It can be argued that the deductions made from simulating the dyn1-PHD on the membrane might be limited in terms of transferability to what could be observed with the full dynamin structure. Though there would be changes, the choice can be justified by looking at some of the experimental work with PHD-mutant or knockouts. In Dar *et al* (1), PHD was replaced by a six residues long His-tag, which affects the fission rate but did not alter any other mechanism of dynamin. Dynamin formed a helix in a similar fashion as it does with WT-PHD. Though tightly coupled to each other, each domain of dynamin has a specific job assigned to it as is the case with most of the multi-domain proteins. Moreover, the sheer size of dynamin makes the computational work prohibitive, even with the largest of computational resource.

3. Effect on bending modulus of membrane due to peripheral protein: Recent article by Fowler *et al* (2) suggests that the contribution of peripheral protein in generating thermal undulation may not be significant enough to affect the bending modulus. The deductions were mostly based on simulations using a small protein tN-Ras. Our results turn out in contrast to the arguments made by the article. Our results show that the shallow-docking peripheral PHDs lower the bending modulus and here could be a couple of possible reasons that could explain this contradiction including the absence of cholesterol which is known to act as a knob to maintain packing "homeostasis" in the membrane. Another crucial factor that supports PHD association is the presence of PIP_2 in our lipid compositions. We observed in our CG simulations (with no PIP_2 molecule in their lipidome), that the PHDs don't stay close to the bilayer for the entire time and some of them actually diffuse long way from headgroup surface. Such behavior was not observed when PIP_2 was added to the system due to the specific binding that occurs between PHD and PIP_2. The other reason could be could be the nature of the protein itself. We would also like to discuss the reduction in bending modulus data in light of several recent studies where different kind of changes in membrane rigidity is observed due to peptides, peripheral and intrinsic proteins. There are several studies where peptides are shown to soften the membrane (3-6) and some very interesting recent work where certain peptides (GWALP in this case) could lead to a liquid-disordered system to have a higher rigidity than ordered systems (7).

4. Spatial distribution of Mean and Gaussian Curvature: We evaluated the spatial distribution of mean and Gaussian curvature for our membrane system, which we describe below. We extracted the co-ordinates of phosphate headgroups of lipids corresponding to one of the leaflets from the coarse-grained simulation systems. And we applied a 2-D Delaunay triangulation algorithm to generate a polygonal mesh of vertices from the co-ordinates of phosphate headgroups. The surface, so generated, was used for evaluating the mean and Gaussian curvature at various vertices of the mesh. We performed these calculations using Python scripts where we used built-in subroutines from the VTK (Visualization ToolKit) library.[8] This same library is used as one of the core modules in Memsurfer.[9] The results were visualized using Paraview[10,11] and its plugins. The Python script developed for the purpose is deposited in the Github repository.

We applied our algorithm on pure membrane and membrane with randomly placed PH Domains. These two systems are discussed in the originally submitted manuscript. To further test for curvature induction, we also created a third system where the PH domains were arranged in double collar – this was done to crudely model the scaffold and with an intention to accentuate the effect of PH Domain on curvature induction. The results for the three system, both for the Gaussian and mean curvature analyses are shown in Fig. R1 and Fig. R2, respectively.

At individual snapshot level, we did not see any noticeable spatial correlation between position of induction of curvatures and position of PH domains. This was true for both mean and Gaussian curvature. It should be noted that the curvatures observed in these membrane systems are quite dynamic in nature. To observe curvatures that are persistent over time (and not simply thermal fluctuations), we performed time-averaging of curvature observed at each point of the membrane surface. Fig. R3 and Fig. R4 show the spatial distribution of time-averaged Gaussian and mean curvatures observed in the CG simulations. We also generated movie files of the trajectories showing the time evolution of curvatures and they are included in in the supporting information as *gaussian-curvature.mp4* and *mean-curvature.mp4.*

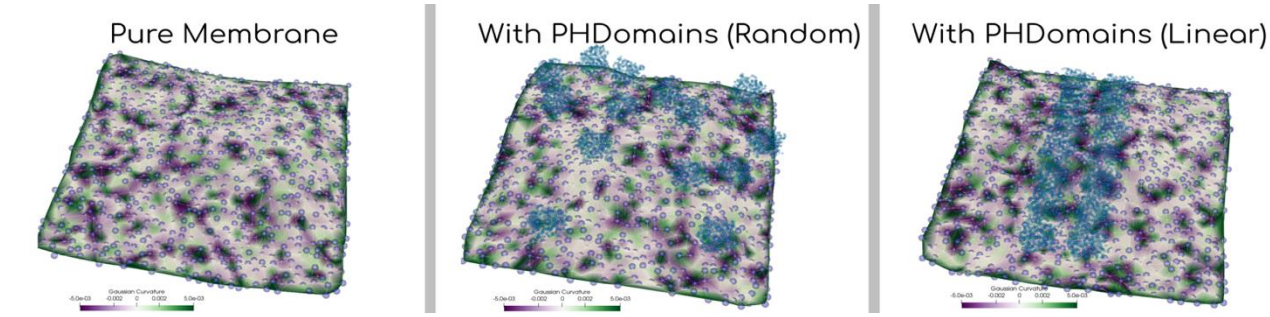

Fig. R1: Single snapshot of Gaussian curvature observed in (a) pure membrane, (b) membrane with randomly placed PH Domains and, (c) membrane with PH Domains arranged in a collar formation.

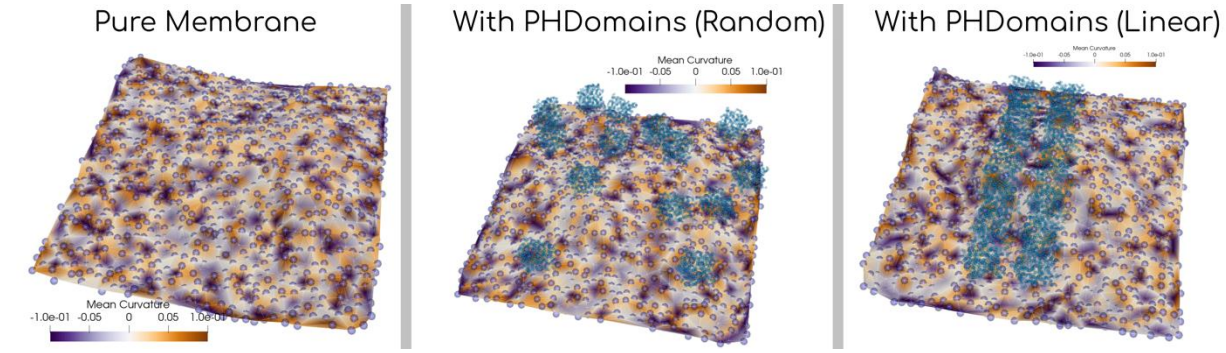

Fig. R2: Single snapshot of mean curvature observed in (a) pure membrane, (b) membrane with randomly placed PH Domains and, (c) membrane with PH Domains arranged in a collar formation.

As seen in Fig. R3, the randomly arranged PH Domain system does exhibit small scattered patches of both positive (Green) and negative (Purple) Gaussian curvatures (though small in magnitude) while pure membrane exhibits predominantly zero curvature (White color). In particular, there is one particular region on the membrane where noticeable Purple patch is seen and this corresponds to the region where a few PH domains are closely positioned. To some extent, this observation suggests that PH domain may be inducing a negative Gaussian curvature (Saddle regions) on the membrane. For the new hypothetical system with PH Domains clustered in a linear arrangement, we can clearly see the presence of persistent patches of both positive and negative Gaussian curvature in systems with PH Domain. We see similar trends for mean curvatures as well (Fig. R4) where most significant changes in curvatures are seen in collar formation. However, we do not find this surprising as the system was designed for an amplified induction of curvatures. Of note, in physiological conditions, the distance between two PH Domains in a dynamin collar is much larger than what we have here. Nevertheless, these analyses shed some important insights into the curvature generation role of PH Domain.

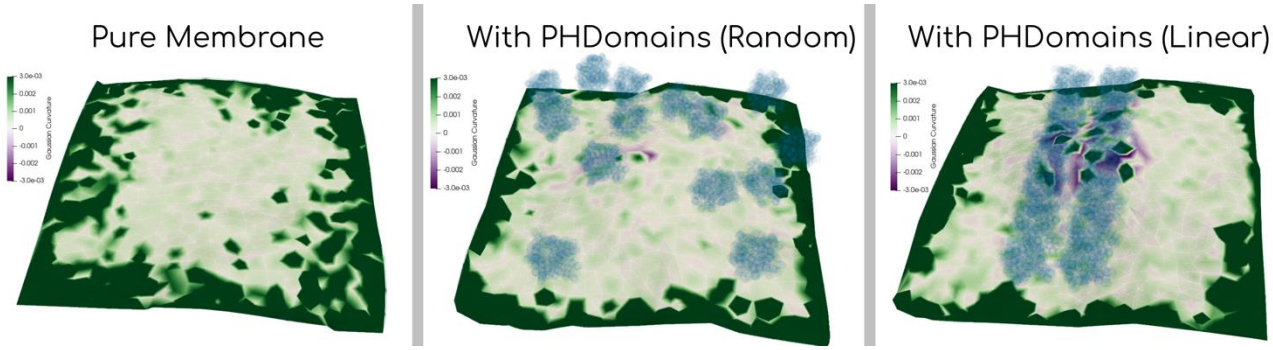

Fig. R3: Time-averaged Gaussian curvature observed in (a) pure membrane, (b) membrane with randomly placed PH Domains and, (c) membrane with PH Domains arranged in a collar formation. The high positive Gaussian on the four edges are artefact of boundary effects and should be ignored.

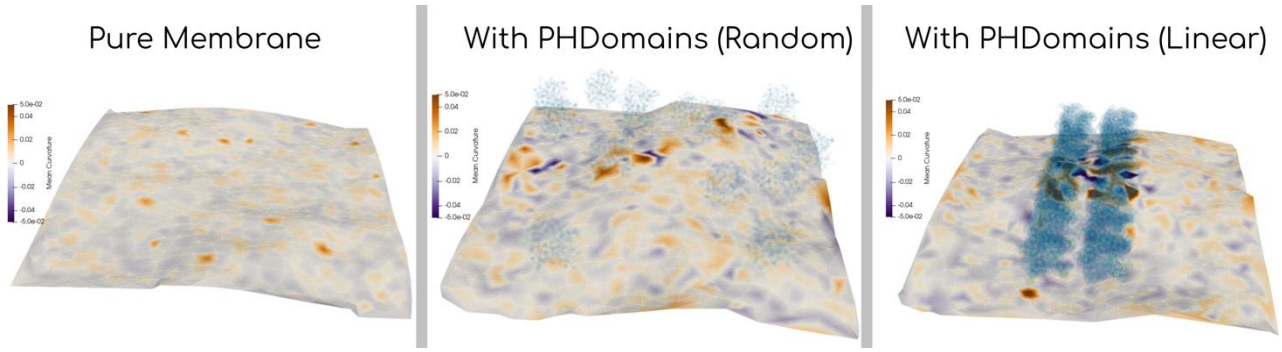

Fig. R4: Time-averaged mean curvature observed in (a) pure membrane, (b) membrane with randomly placed PH Domains and, (c) membrane with PH Domains arranged in a collar formation.

References:

1. Dar S & Pucadyil TJ (2017) The pleckstrin-homology domain of dynamin is dispensable for membrane constriction and fission. *Molecular biology of the cell* 28(1):152-160.

2. Fowler PW, *et al.* (2016) Membrane stiffness is modified by integral membrane proteins. *Soft Matter* 12(37):7792-7803.

3. Tristram-Nagle S, *et al.* (2010) HIV fusion peptide penetrates, disorders, and softens T-cell membrane mimics. *Journal of molecular biology* 402(1):139-153.

4. Pott T, Gerbeaud C, Barbier N, & Méléard P (2015) Melittin modifies bending elasticity in an unexpected way. *Chemistry and physics of lipids* 185:99-108.

5. Dimova R (2014) Recent developments in the field of bending rigidity measurements on membranes. *Advances in colloid and interface science* 208:225-234.

6. Pabst G, Danner S, Podgornik R, & Katsaras J (2007) Entropy-driven softening of fluid lipid bilayers by alamethicin. *Langmuir* 23(23):11705-11711.

7. Usery RD, *et al.* (2018) Membrane Bending Moduli of Coexisting Liquid Phases Containing Transmembrane Peptide. *Biophysical journal* 114(9):2152-2164.

8. Schroeder, Will J., Bill Lorensen, and Ken Martin. *The visualization toolkit: an object-oriented approach to 3D graphics*. Kitware, 2004.

9. Bhatia, Harsh, et al. "MemSurfer: a tool for robust computation and characterization of curved membranes." *Journal of chemical theory and computation* 15.11 (2019): 6411-6421.

10. Ahrens, James, Berk Geveci, and Charles Law. "Paraview: An end-user tool for large data visualization." *The visualization handbook* 717.8 (2005).

11. Bethel, E. Wes, Hank Childs, and Charles Hansen, eds. *High performance visualization: Enabling extreme-scale scientific insight*. CRC Press, 2012.